Hindawi
Mathematical Problems in Engineering
Volume 2018, Article ID 2850309, 10 pages
https://doi.org/10.1155/2018/2850309

Research Article

Modal Analysis of a New Thermosensitive Actuator Design for Circuit Breakers Based on Mesoscale U-Shaped Compliant Mechanisms

Horacio Ahuett-Garza,[1] **Juan I. Melecio**,[2] **and Pedro Orta**[1]

[1] *Tecnologico de Monterrey, Escuela de Ingeniería y Ciencias, Monterrey, Mexico*
[2] *Power Conversion Group, School of Electrical and Electronic Engineering, The University of Manchester, UK*

Correspondence should be addressed to Horacio Ahuett-Garza; horacio.ahuett@itesm.mx

Received 24 February 2018; Revised 8 June 2018; Accepted 25 June 2018; Published 16 July 2018

Academic Editor: Ivano Benedetti

A new mesoscale thermosensitive actuator design for circuit breakers based on a U-shaped compliant mechanism was introduced as a potential replacement for bimetal strips in miniature circuit breakers. In a previous study, the response of this design to the thermal fields produced by a steady current flow was analyzed. This article presents a modal analysis of the compliant mechanism. The goal of the analysis is to compare the natural frequencies of the mechanism with the frequency of the magnetic loads caused by the flow of the alternating currents. Simulations with simple beam elements and 3D elements are presented and results are compared with experimental measurements. The study finds that the natural frequency of the mechanism differs by a factor of about 8 with the AC frequency. The conclusion is that the proposed compliant mechanism design's performance as a thermal actuator will not be affected by the cyclic loads generated by the forces induced by the AC magnetic fields.

1. Introduction

Miniature circuit breakers (MCB) are a vital element for the protection of electric circuits against power surges. Their main function is the interruption of current flow as a protective measure against potentially dangerous conditions, such as overloads and short circuits. Currently, common electromechanical MCB designs in the market use a bimetal strip as a key element of the thermal trip system. The patent for the basic MCB design that relies on bimetal technology was originally granted in 1959 [1]. Although new trip mechanism designs have been developed since then [2, 3], bimetal strip-based technology is still the most widely used because of its low cost, high reliability, and robustness.

Figure 1 shows the mechanisms of the circuit breaker that was used as a starting point for the proposed design. The breaker contains two different trip systems which provide the current interruption actions in a coordinated manner. The thermal trip unit protects against current overloads, and the electromagnetic unit interrupts current flow when short circuits or sudden power surges occur. A bimetal strip is the main actuator of the thermal unit, while an armature provides the quick response to sudden power surges. Current flows only through the bimetal strip, and overloads result in a temperature rise, which causes the bimetal to deflect. This in turn pulls down the yoke and the armature, releasing the trip lever. In the magnetic trip system, a short circuit results in large current flow, which in turn induces a strong magnetic field. This field induces a force on the armature, which deflects in consequence, thus releasing the trip lever. Current overloads are relatively slow events that may develop in spans of minutes. On the other hand, short circuits occur in a fraction of a second, and the MCB mechanism should ideally act in about a quarter of an AC cycle (4.17 milliseconds for a 60 Hz AC source).

From the previous discussion, the bimetal strip is critical for the performance of the circuit breaker. The bimetal strip is expected to deflect under the thermal loads produced by the current flow. At the same time, it is expected to provide stable support for the armature. In operation, the mechanism

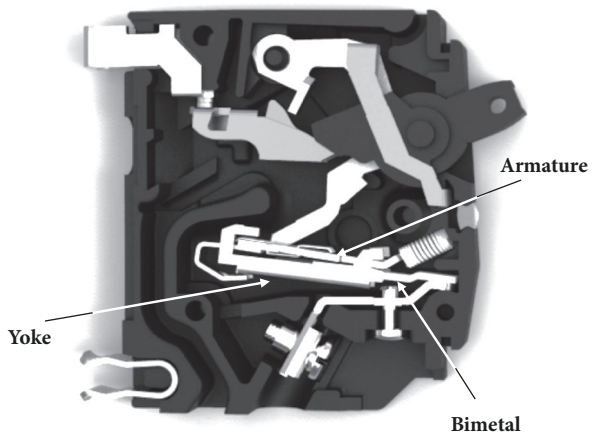

Figure 1: Internal view of conventional MCB trip mechanisms equipped with the bimetal strip.

is subjected to cyclic loads caused by the alternating currents that flow through it. This requires the mechanism to be insensitive to the forces caused by the magnetic fields that are in turn induced by the fluctuating current.

A new mesoscale compliant mechanism design was proposed as a potential replacement for bimetal strips in MCB. The proposed design is based on a U-shaped compliant mechanism and performs the two basic functions: the trip action for overload conditions and support for the magnetic trip system. Prototypes of the mechanism were tested under normal, overload, and short circuit conditions, and their performance in these tests met the requirements defined by industrial standards. The interest in the new design arises from the potential it has to reduce energy losses in the breaker [4].

The functions that the mechanism performs pose a challenging design problem: the mechanism structure must be designed to deflect under thermal loads of a certain magnitude, while providing firm support to a second structure in presence of a varying force field. The previous work focused only on quasi static conditions. To validate the performance of the mechanism under the fluctuating magnetic fields, a modal analysis of the design was conducted. Finite element (FE) models of the mechanism were prepared using three different formulations: frame elements in a simple code developed for quick analysis, 3D Hexahedron elements, and 3D beam elements of Altair OptiStruct commercial solver software. There are two particular objectives of this study. The first one is to establish the capacity of the mechanism to be insensitive to the forces induced by the varying magnetic fields. The second one was to test the suitability of different mathematical models to predict this behavior, in particular the code that uses the 2D frame formulation. The development of code for quick analysis is of interest given the increasing computing capabilities of portable computers and mobile devices. A particularity of this work is related to the size of the compliant mechanism. A significant amount of work can be found in the literature for micro- and nanoscale mechanisms. Few studies are available for mesoscale applications.

This article is organized as follows. Section 2 presents a review of the literature. Section 3 describes the compliant mechanism design. The modeling procedure is introduced in Section 4 for the case of 2D modes. Section 5 presents the simulation results, and the experimental tests are presented in Section 6. Results are discussed in Section 7. Finally, conclusions and future work are presented in Section 8.

2. Literature Review

There are a number of studies of the behavior of flexures used as thermoactuator under steady state conditions, particularly for micromechanical applications. Guckel et al. [5] proposed the basic architecture of a family of compliant actuators that could bend under the effect of magnetic fields or thermal loads flexures for microswitching operations. Even though their proposal applied to microscale actuators, their design inspired the design presented in this work. Jonsmann et al. [6, 7] presented a series of thermoactuators that could be built by laser micromachining or electroplating. They used topology optimization techniques to produce the designs. A metallic flexure was tested and its deflection under the action of small currents was measured. Luo [8] compared the response of a flexure of a similar design, made of different materials, nickel and poly-Si. Flexure deflection caused by the thermal fields induced by constant currents was predicted with FE models. Results were compared to experimental measurements. Colbert et al. [9] conducted a review of the literature for thermoactuated flexures and developed models for the response of U-shaped flexures under steady state conditions. From the perspective of design methodologies, Zhao et al. [10] report the use of topology optimization, while Ansola et al. [11] used forward topology optimization thermocompliant mechanisms.

The response of compliant mechanisms to dynamic loads has also received a lot of attention. The two common approaches to characterize a flexure design are to obtain the natural frequencies by modal analysis and to perform direct measurements. A few studies have focused on developing methodologies to predict natural frequencies of compliant mechanisms. In an early work, Lyon et al. [12] used the pseudo rigid model to predict the first modal value of four configurations of parallel motion compliant mechanisms. Yu et al. [13] developed a more general methodology to predict natural frequencies of compliant mechanisms using dynamic equivalency and the pseudo rigid body model. Xu [14] analyzed a long stroke micropositioner that uses leaf type flexures and compared natural frequencies of FE models versus analytic models. Results were within 12%. The analytic models were based on the pseudo rigid models for beam type compliant mechanisms developed by Howell. Topology optimization techniques have also been applied to the analysis of compliant thermoactuators. Ansola et al. [11] worked on models with spatial varying thermal fields.

Most studies, however, focus on specific designs. As a consequence, there are a vast number of reports, particularly in the field of microelectric machine (MEMs) design. For

example, Qi et al. [15] compared the natural frequencies of alternate designs of a bridge type amplifying planar mechanism. Li and Xu [16] introduced a planar parallel compliant stage and developed a matrix-based compliance/stiffness lumped model to predict stage deformations and natural frequencies with FE models. Natural frequencies predicted by the matrix model lay within 10% of the FE results for the first three frequencies. Tian et al. [17] used a similar methodology, i.e., lumped mass spring model and 3D FE, for a different nanopositioner design. Reported natural frequencies are virtually the same for both models and match well with experimental results. Predicted response under quasi static loads was not as accurate. The authors attribute the discrepancy to the inaccuracy associated with the hinge models. Polit et al. [18] theoretical models reported that deviations between FE and lumped models are about 5%. Tian et al. [17] presented an experimental study of the dynamic behavior of a positioner for grinding operations. The design of the mechanism is interesting because it is a three-dimensional structure, as opposed to the more conventional planar designs.

The design of circuit breakers and fault protection systems is critical for power transmission. A significant amount of work is available in the literature. Recent interest centers on Direct Current (DC) applications. To name but a few, Kulkarni et al. [19] looked at the use of AC circuits breakers with reactors for protection of DC circuits, and Mokhberdoran et al. [20] designed solid state breakers for the DC circuits. More related to the work in this article, Deb et al. [21] analyzed and classified the toggle mechanisms used in circuit breakers. Their goals were to improve the tools available for the systematic design of electric switches and explore the potential application of new designs and concepts.

Several studies have looked at compliant mechanism design at the mesoscale. The consensus about dimensions considered mesoscale varying for different applications. For the purposes of this work, the definition proposed by Valdastri et al. [22] is used. They consider mesoscale when a mechanism size lies in the range of tenths of millimeters to tenths of centimeters. Their work focused on the design of compliant legged locomotion systems for biomedical applications. Varma et al. [23] used piezoelectric actuators with compliant mechanisms to amplify the range of motion of a mesoscale positioning system. In both cases, the size of the final components was a few centimeters, but neither work characterized the dynamic behavior of the compliant element. York et al. [24] designed an actuator 8 mm in length, with a travel range of a few hundredths of a millimeter. A transient response analysis was also conducted, in preparation for high speed actuation applications.

In summary, a significant amount of work for the characterization of the dynamic response of compliant mechanisms for micro- and nanoscale applications is available. The literature for mesoscale applications is not nearly as abundant. The application of thermoactuated compliant mechanisms for circuit breaker design offers the opportunity to improve the understanding of the dynamic behavior of mesoscale compliant mechanisms. The rest of the article presents an analysis of a novel, mesoscale compliant mechanism and the experimental work that validates the analysis.

3. Design of Compliant Mechanism

In the current case, a compliant mechanism U-shaped design was proposed as a solution to meet the design criteria. As explained before, the response of this shape to different types of loads has been reported in the literature, particularly for microactuating applications [5–9]. The design goal for the compliant mechanism was to replace the bimetal strip without affecting the rest of the breaker design, not only in terms of function but also regarding the available spaces within the MCB box. The basic shape is shown in Figure 2. Each one of the arms of the U has a different cross-sectional area. A current flowing through them will produce a temperature difference between the two arms and thus a different expansion of each arm. This causes the whole compliant mechanism to bend under the influence of the thermal fields. Equation (1) describes the relationship between the intensity of the current and temperature rise in the conductor.

$$\Delta T = \int_0^t \frac{Ri\,(t)^2}{mc} dt \tag{1}$$

In (1), i(t) is the current as a function of time, m and R are the mass and resistance of the conductor material and can be obtained from $m = \rho V$ and R= r_y ∗lg/bd, where ρ is the density, r_y is the resistivity of the material, V is the conductor's volume, lg is the length of the conducting arm, b is the depth of the conductor, and d is its height. Melecio et al. [4] present the details of the derivation of (1).

Given that the basic topology was prescribed, the design task consisted first in establishing a cross section to perimeter ratio in such a way that the temperature rise caused by the current flow could be kept within specified limits. The next step was to calculate the actual dimensions of the cross section to guarantee a certain deflection under the said temperature rise. As shown in Figure 2, a slight curvature (curvature radio of 620mm) was added to one of the legs to force the mechanism to deflect in a specific direction, consistent with the magnitude of the temperature variation. The free arm is intended to replace the bimetal strip of the conventional MCB design and functions both as actuator for tripping under overload conditions and as support for the armature. Proper use of the anchor points rounds the design.

A prototype MCB box equipped with the compliant mechanism is shown in Figure 3. For this particular design, a temperature rise of about 90°C results in a 0.95 mm deflection of the free end, enough to cause the thermal protection to trip. Under these conditions, the thermal overload protection provided by the compliant mechanism is very similar to the performance of the bimetal strip. A full explanation of the design process and the performance under overload conditions can be found in [4].

The compliant mechanism is made out of aluminum. In the analysis that follows, all cases assume the use of aluminum with the properties shown in Table 1.

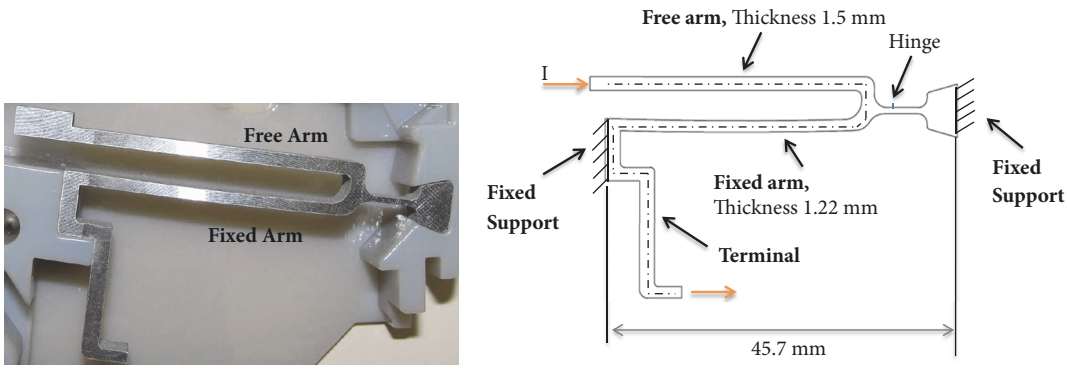

Figure 2: (a) U-shaped thermosensitive compliant mechanism. (b) Dimensions of mechanism.

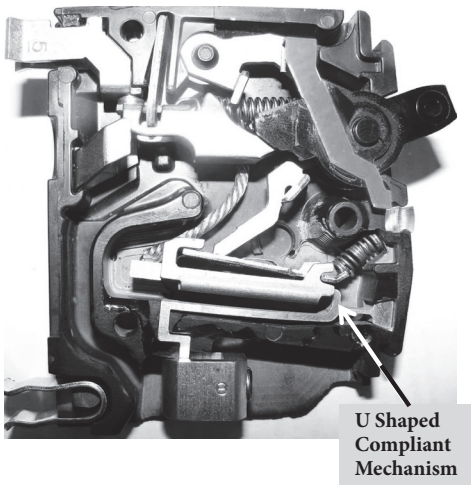

Figure 3: Internal view of prototype MCB, equipped with compliant mechanism that replaces bimetal strip.

Table 1: Material properties for aluminum used in the simulations.

Young's Modulus	68.9 Gpa
Poisson's Ratio	0.33
Density	2800 kg/m3

4. Modal Analysis with Plane Frame Elements

The goal of the analysis is to establish the suitability of the design to provide support to the armature under the fluctuating magnetic fields. Specifically, the natural frequencies of the mechanism have to be significantly different from those found in current power systems (50–60 Hz) for the mechanism to be considered insensitive to the forces induced by the magnetic fields.

An FEA program was written for quick analysis of structures using plane frame elements using Mathematica. The program can calculate displacements caused by static loads or by predetermined temperature variations of the frame elements. It also calculates the natural frequencies of the structure. A preprocessor generates a mesh from data that can be input manually or in a table. A postprocessor displays the deflection data as well as the deflection patterns or mode shapes, depending on the type of analysis.

For the modal analysis, the system to solve is an eigenvalue problem of the form

$$([K] - \lambda [M]) = 0 \tag{2}$$

The matrices are constructed using a consistent formulation with the Galerkin method [25], in which cubic polynomials and their derivatives are used to interpolate transverse displacements and rotations, and linear functions are used to interpolate axial displacements. A brief description of the derivation is shown in the Appendix. Although the program used in this work performs numerical integration to calculate the actual element stiffness and mass matrices, it can be shown that the terms of the stiffness matrix [K] for a frame element are

$$[\mathrm{K}] = \begin{bmatrix} c_1 & 0 & 0 & -c_1 & 0 & 0 \\ 0 & 12c_2 & 6h_e c_2 & 0 & -12c_2 & 6h_e c_2 \\ 0 & 6h_e c_2 & 4h_e^2 c_2 & 0 & -6c_2 & 2h_e^2 c_2 \\ -c_1 & 0 & 0 & c_1 & 0 & 0 \\ 0 & -12c_2 & -6h_e c_2 & 0 & 12c_2 & -6h_e c_2 \\ 0 & 6h_e c_2 & 2h_e^2 c_2 & 0 & -6h_e c_2 & 4h_e^2 c_2 \end{bmatrix} \tag{3}$$

where

$$c_1 = \frac{EA}{h_e}$$
$$c_2 = \frac{EI}{h_e^3} \tag{4}$$

And E is Elastic Modulus, A is cross sectional area of beam element, I is moment of area, and he is the characteristic

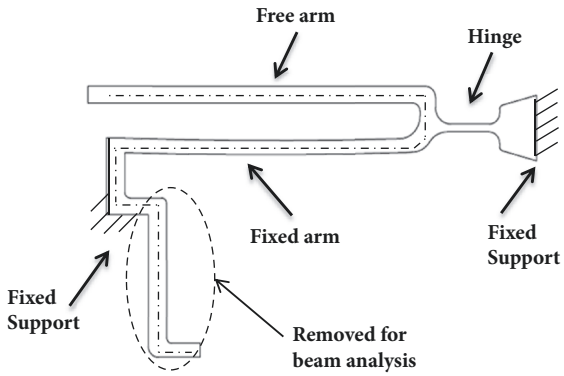

Figure 4: Model used for FE analysis. A section is removed for beam and 2D models.

element length. Similarly, it can be shown that the matrix [M] for an element is defined as

$$[M] = \frac{\rho A h_e}{420}\begin{bmatrix} 140 & 0 & 0 & 70 & 0 & 0 \\ 0 & 156h_e & 22h_e & 0 & 54 & -13h_e \\ 0 & 22h_e & 4h_e^2 & 0 & 13h_e & -3h_e^2 \\ 70 & 0 & 0 & 140 & 0 & 0 \\ 0 & 54 & 13h_e & 0 & 156h_e & -22h_e \\ 0 & -13h_e & -3h_e^2 & 0 & -22h_e & 4h_e^2 \end{bmatrix} \quad (5)$$

The order of the matrix is 3n x 3n, where n is the number of nodes for which a solution is sought. Once a mesh is developed and the corresponding matrices are constructed, a standard Mathematica routine for eigenvalue solution was used to establish the natural frequencies.

5. Finite Element Modal Analysis of Compliant Mechanism for MCB

The dimensions of the compliant mechanism are shown in Figure 2(b). Dimensions range from as little as 0.6 mm for the hinge to 45.7 mm in length of the mechanism. As can be seen in the figure, the free arm is slightly thicker than the fixed arm. As a consequence, temperature increases more in the fixed arm, which causes the free arm to deflect depending on the temperature differential of both arms. A very slight curvature (radius of curvature of 620 mm) is given to the fixed arm to guarantee deflection in the correct direction. Figure 4 shows the geometry with the boundary conditions used in the modal analysis.

The mesh for the 2D frame elements model of the flexure is shown in Figure 5(a). The hinge was modeled as a beam. It is important to note that Element 8 in the mesh is actually thicker than the rest of the beam. This is needed to provide a better representation of the actual compliant mechanism, in which a thicker section was manufactured to provide space for electrical connections. Beam cross sections were modified at 4 different flexure sections to represent the rest of the geometry. Figures 5(b) and 5(c) show the first two modes and natural frequencies. The formulation for these models was presented in the previous section.

Table 2: Convergence analysis, truss element model.

# of Elem.	1st Nat. Freq. (Hz)	2nd Nat. Freq. (Hz)
11	450.942	2789.51
14	450.789	2659.01
17	450.788	2658.76
19	450.788	2658.76
21	450.788	2658.68
22	450.788	2658.68

Table 3: Convergence analysis, CBEAM elements.

# of Elem	1st Nat. Freq. (Hz)	2nd Nat. Freq. (Hz)
22	438	2673
44	439	2630
88	440	2634

Table 4: Convergence analysis, CHEXA elements.

# of Elem	1st Nat. Freq. (Hz)	2nd Nat. Freq. (Hz)
1055	553	3131
7560	528	3043
20692	520	2994
56180	516	2980

The results of the convergence analysis for this mechanism is presented in Table 2.

The same geometry was analyzed using Altair Hypermesh for model preparation and OptiStruct as solver. As mentioned before, two different types of elements were used, beam elements and hexahedral elements.

Three-dimensional CBEAM type beam elements were used in the first model. The convergence analysis for this case is shown in Table 3, and the first two in-plane mode shapes are shown in Figure 6.

Three-dimensional CHEXA type elements were used in the second model. The convergence analysis for this case is shown in Table 4, and the first two in-plane mode shapes are shown in Figure 7.

Clearly, in the case of the beam models, all modes are in the plane. In the case of the three-dimensional CHEXA model, the second mode shape showed deformation in the direction of the width, out of the plane.

6. Experimental Validation

The natural frequencies of the compliant mechanism were measured using a Polytec vibrometer Model CLV-2534. Two aluminum prototypes of the compliant mechanism were tested. In each test, a mechanism was clamped at two points on a vice, as shown in Figure 8(a). An impact hammer was used to cause an excitation in the mechanism, and deflections were recorded by the system.

Figure 9 shows data for one of the two tests. Two natural frequencies can be observed, the first one at approximately

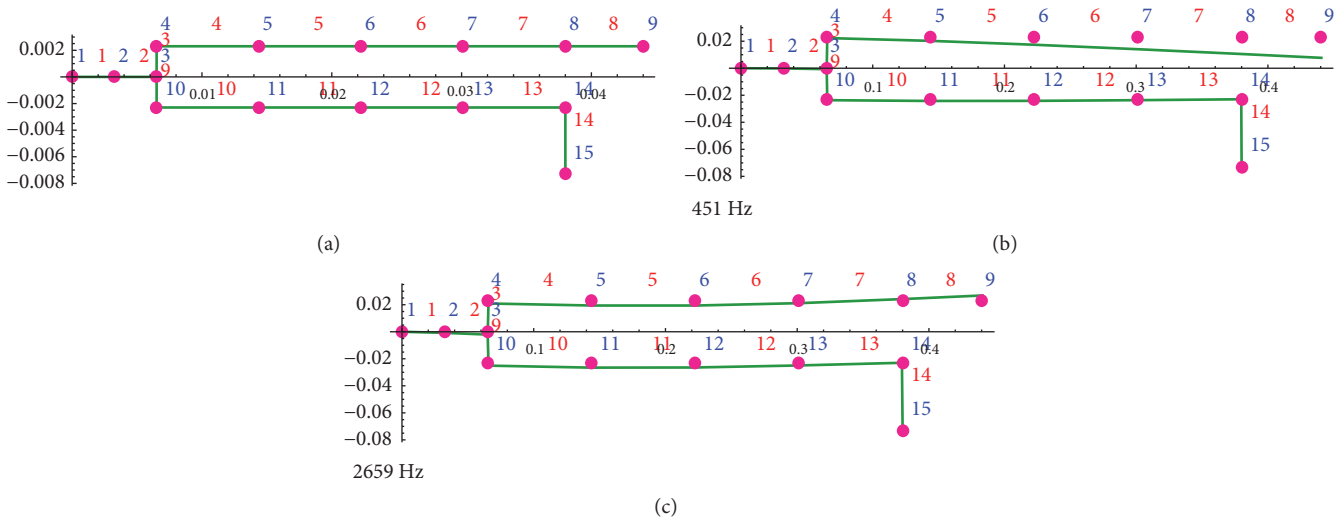

Figure 5: (a) Two-dimensional frame element model. (b) First and (c) second natural frequencies and mode shapes.

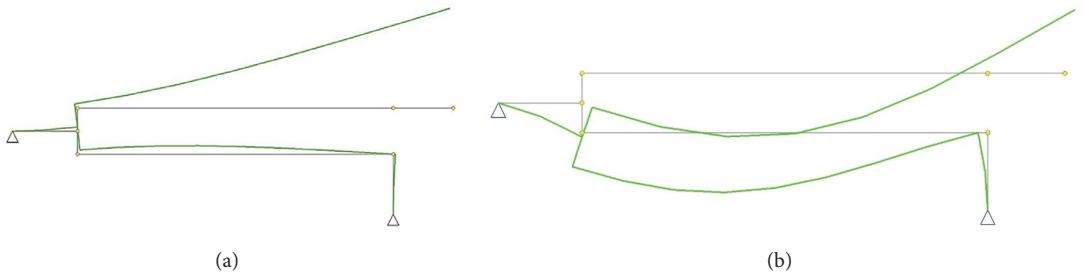

Figure 6: Shape modes with CBEAM type elements. (a) First mode. (b) Second mode.

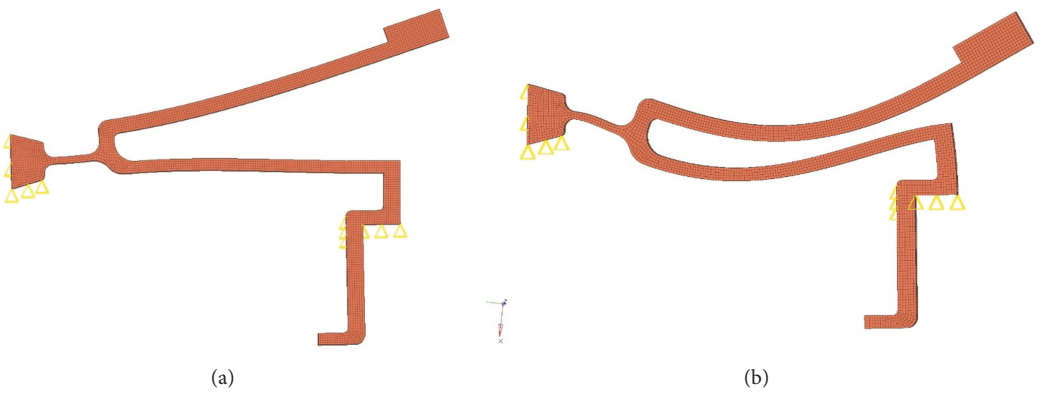

Figure 7: Mode shapes. (a) First mode. (b) Second mode, 3D hexahedron model, and commercial system.

440 Hz and the second one at 2673 Hz. Because of probe alignment in the experimental setup, only vertical deflections are measured.

7. Results and Discussion

Table 5 summarizes the results of all cases: each experiment and simulation results with two-dimensional (2D) frame elements, as well as the 3D beam elements and three-dimensional (3D) and hexahedral elements.

As can be seen, there is a very good match between the simulation results and the experimental data for the case of the frame and beam elements. The difference in the first two natural frequencies was less than 2.5%. The hexahedral element results were less accurate, with a difference of almost 18% in the worst case. The probable reason is that hexahedral elements tend to be numerically stiffer, and as a consequence the natural frequencies tend to be overestimated.

From the perspective of the performance of the compliant mechanism, line frequencies are in the 50 to 60

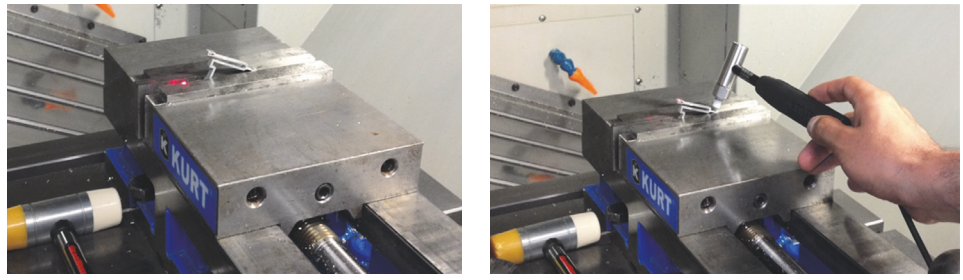

(a) (b)

Figure 8: Experimental setup (a) compliant mechanism in clamped position. (b) Impact hammer and laser sensor just prior to test.

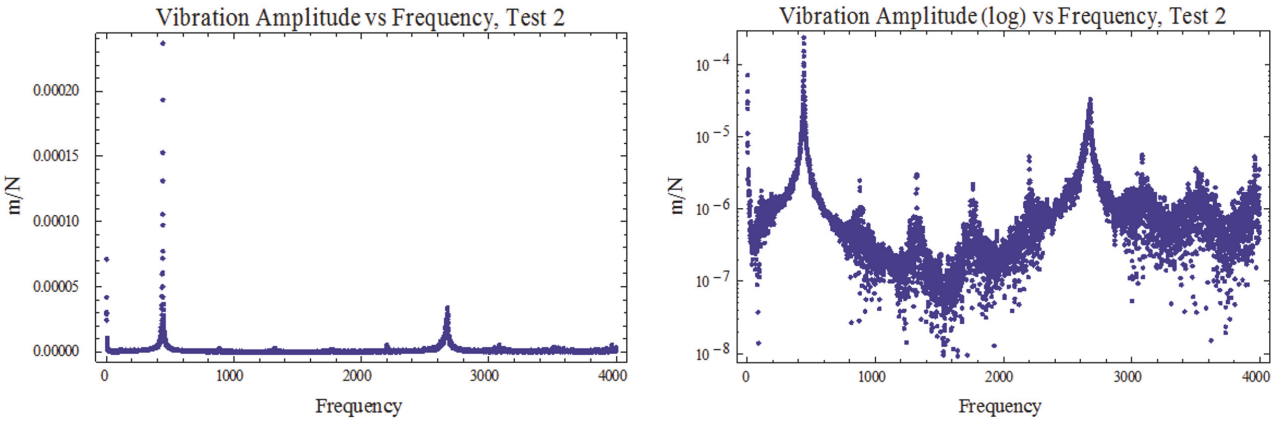

(a) (b)

Figure 9: Scatter plots of the vibration tests. (a) Linear scales that highlight the first two natural frequencies in the plane. (b) Log scales, where harmonics can be identified.

Table 5: Comparison of results.

Natural Frequency	Exp 1 (Hz)	Exp 2 (Hz)	2D Frame Elements	3D Beam Elements	3D Hexahedral Elements
1	440.625	440.625	451	440	516
2	2676.25	2678.75	2659	2634	2980

Hz, depending on the geographical location. Ideally, the excitation frequency should be much larger than the natural frequency of the system, making the system insensitive to the excitation. For the case of the North American households, the magnetic fields fluctuate at 60 HZ, which is about 15% of the natural frequency of the mechanism. That is, frequencies at normal operating conditions are significantly different from the natural frequencies.

Under normal conditions, the forces produced by the magnetic fields are relatively small. Experimental data for forces or deflections induced by the magnetic fields in MCB, of this or similar designs, is not available. However, simulation results [26] suggest that the force induced by the magnetic field on the yoke would be in the range 0.08N for overload conditions (60A). Experiments with the conventional mechanism have shown that a force of about 0.35 N is needed to trip the armature [26]. If the natural frequencies of the compliant mechanism matched those of the line, it is unlikely that the proposed design would pass the overload test, given that per standards the trip mechanism must allow overloads for short periods of time. Lab tests of prototype MCB's equipped with the compliant mechanism have shown that performance meets the standards, even for overload conditions. This behavior is consistent with the conclusions that can be drawn from the modal analysis.

8. Conclusions

This work presented a modal analysis of a new mesoscale thermosensitive actuator design for circuit breakers based on a U-shaped compliant mechanism. The study was necessary to provide a full characterization of the proposed design. The results of different FE models were compared to the results of experimental tests, and a very good match was found. Overall, the results of this study are consistent with the performance of prototype MCB in lab tests.

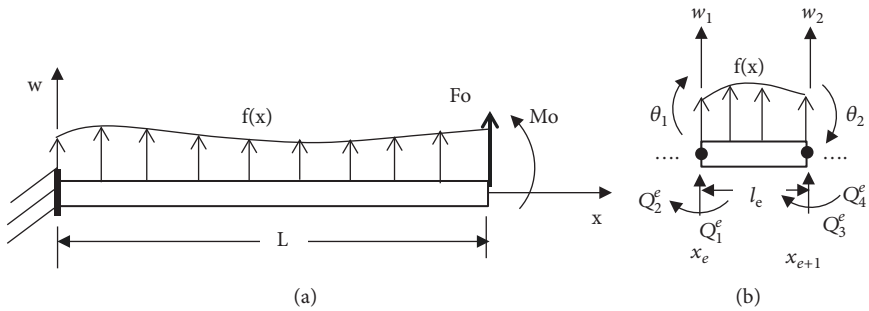

Figure 10: Fixed beam with loads. (a) Basic problem and (b) beam element.

This work has highlighted the capacity of simple computer models to provide valuable information about particular compliant mechanism designs, a very valuable capacity during early stages of design, in which candidate geometries are compared. Another contribution of this work is the analysis and supporting experimental data for the behavior of a mesoscale compliant mechanism. While significant work has been done on micro- and nanoscale compliant mechanism, data for mesoscale applications is much scarcer.

A few directions for future work are being explored. The development of other compliant mechanism configurations for different MCB protection designs is being explored, as well as the potential use of these configurations for similar applications such as thermal-mechanical overload relay design. Also, the use of 2D beam elements lends itself to combination with other techniques, such as neural networks, to speed up iterations at early stages of the design process. The code presented here is currently being tested for developments using this approach.

Appendix

A. Formulation Used in Frame Element Program

This section presents a brief explanation of the formulation used in the frame element FE program. A number of excellent books provide an in-depth explanation of the technique. Most of the current explanation can be found in specialized literature, such as Reddy [25]. In the Euler-Bernoulli beam element, shown in Figure 10, the transverse deflection w is governed by the following equation:

$$\frac{d^2}{dx^2}\left(b\frac{d^2w}{dx^2}\right) = f(x) \quad for\ 0 < x < L \tag{A.1}$$

For beams, b = EI, where E is the Elastic Modulus of the material, and I is the moment of area of the cross section of the beam.

A finite element formulation proposes a solution of the weak form of the previous equation. The basic idea is to discretize the domain in elements (Figure 10(b)) and device a solution over each element, which must be consistent over the mesh of elements that makes up the full geometry. The approach produces the same results as a weighted residual method. Over the element, a solution for w is sought in such a way that the weak form is solved:

$$0 = \int_{x_e}^{x_{e+1}} v\left[\frac{d^2}{dx^2}\left(b\frac{d^2w}{dx^2}\right) - f(x)\right]dx \tag{A.2}$$

where v is a function that is twice differentiable. Integration by parts results in

$$\begin{aligned} 0 = &\int_{x_e}^{x_{e+1}} \left(b\frac{d^2v}{dx^2}\frac{d^2w}{dx^2} - vf\right)dx \\ &+ \left[v\frac{d}{dx}\left(b\frac{d^2w}{dx^2}\right) - \frac{dv}{dx}b\frac{d^2w}{dx^2}\right]_{x_e}^{x_{e+1}} \end{aligned} \tag{A.3}$$

The terms in the integral are used to construct the stiffness matrix that characterizes the particular geometry, while the term in the bracket represents the essential boundary conditions (deflection and slope) and natural boundary conditions (shear and moment).

An approximate solution for w over the element is proposed in the finite element model:

$$W^e = \sum_{i=1}^{n} u_i^e \emptyset_i^e \tag{A.4}$$

where u_i^e represent the nodal values of the solution and $\emptyset_i^e$ are the approximate functions over the element. These functions must meet certain requirements for continuity and completeness. The finite element provides a structured way to select these functions. In our case, Hermite interpolation functions were used:

$$\emptyset_1^e = 1 - 3\left(\frac{\overline{x}}{h_e}\right) + 2\left(\frac{\overline{x}}{h_e}\right)^3 \tag{A.5}$$

$$\emptyset_2^e = -\overline{x}\left(1 - \frac{\overline{x}}{h_e}\right)^2 \tag{A.6}$$

$$\emptyset_3^e = 3\left(\frac{\overline{x}}{h_e}\right)^2 - 2\left(\frac{\overline{x}}{h_e}\right)^3 \tag{A.7}$$

$$\emptyset_4^e = -\overline{x}\left[\left(\frac{\overline{x}}{l_e}\right)^2 - \frac{\overline{x}}{l_e}\right] \tag{A.8}$$

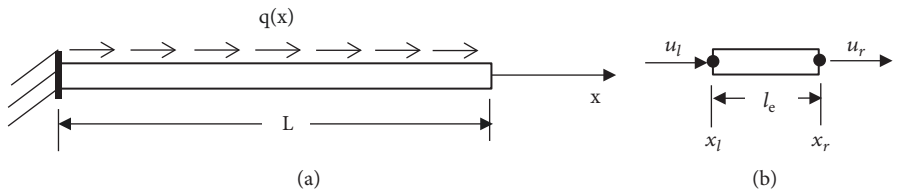

Figure 11: Truss with loads. (a) Basic problem and (b) beam element.

where $\overline{x} = x - x_e$ is the coordinate within the element and $h_e = x_{e+1} - x_e$ or the length of the element. Furthermore, in the Galerkin method used in our formulation, the same functions used for the approximation W^e are used for the weight function v. Plugging (A.5) through (A.8) in (A.3) results in

$$0 = \sum_{j=1}^{4} K_{ij}^e u_j^e - F_i^e \tag{A.9}$$

where

$$K_{ij}^e = \int_0^{l_e} \left(EI \frac{d^2 \emptyset_i^e}{dx^2} \frac{d^2 \emptyset_j^e}{dx^2} \right) dx \tag{A.10}$$

And

$$F_i^e = \int_0^{l_e} \emptyset_i^e f \, dx + Q_i^e \tag{A.11}$$

is the term for the forces acting on the beam. Note that b in (A.2) has been replaced by EI for the beam problem, and Q_i^e accounts for the forces and moments at the boundary of (A.3). K_{ij}^e constitute the elements of the stiffness matrix for the element, which is 4 x 4 for the Euler–Bernoulli formulation. Also, notice that i and j take values 2, 3, 5, and 6, when establishing the factors of the frame element matrix. That is, the parameters K_{ij}^e of (A.10) are placed in the spaces that are left in matrix [K] of the main body that do not belong to rows and columns 1 and 4. Care must be taken to avoid mixing the elements. For example, term $[K_{3,3}]$ in the matrix actually corresponds to term $K_{2,2}^e$; that is,

$$K_{22}^e = \int_0^{l_e} \left(EI \frac{d^2 \emptyset_2^e}{dx^2} \frac{d^2 \emptyset_2^e}{dx^2} \right) dx \tag{A.12}$$

where

$$\frac{d^2 \emptyset_2^e}{dx^2} = -\frac{2}{h_e} \left(\frac{3\overline{x}}{h_e} - 2 \right) \tag{A.13}$$

By plugging (A.13) into (A.12) and solving, the correct term is obtained $(4EI/h_e)$.

The remaining elements of the 6 x 6 fame element [K] come from the solution of the beam under tension forces, shown in Figure 11:

$$0 = -\frac{d}{dx} \left(EA \frac{du}{dx} \right) - q \quad for \ 0 < x < L \tag{A.14}$$

where u is the axial deflection of the bar. Using the same procedure, the weak form is developed as

$$0 = \int_{x_l}^{x_r} v \left[-\frac{d}{dx} \left(EA \frac{du}{dx} \right) - q \right] dx \tag{A.15}$$

For an element, after integration

$$0 = \int_{x_l}^{x_r} \left(EA \frac{dv}{dx} \frac{du}{dx} - vq \right) dx - \left[vEA \frac{du}{dx} \right]_{x_l}^{x_r} \tag{A.16}$$

Again, the term in brackets account for conditions at the boundary. Assuming a solution of the form

$$U^e = \sum_{i=1}^{n} c_i^e \emptyset_i^e \tag{A.17}$$

functions in this case are

$$\emptyset_1^e = 1 - \frac{\overline{x}}{l_e}, \qquad \emptyset_2^e = \frac{\overline{x}}{l_e} \tag{A.18}$$

Elements of the stiffness matrix for this case are

$$K_{gm}^e = \int_0^{l_e} \left(EA \frac{d\emptyset_g^e}{dx} \frac{d\emptyset_m^e}{dx} \right) d\overline{x} \tag{A.19}$$

As before and referring to the main body of the article, [K] matrix elements (1,1), (1,4), (4,1), and (4,4) are defined by elements $K_{1,1}, K_{1,2}, K_{2,1}, K_{2,2}$ from (A.19), respectively. As a final note, a similar procedure in which the same functions are used to develop the mass matrices was followed for consistency.

Nomenclature

E:	Elastic Modulus
I:	Moment of area of cross section
A:	Area of cross section
L:	Length of beam
he:	Characteristic element length
w:	Transverse deflections
u:	Longitudinal deflections
f:	Force function
q:	Traction function
Fo and Mo:	Applied force and moment
θ:	Angular deflection of beam
ø:	Interpolation functions
i(t):	Current as a function of time
m:	Conductor's mass
R:	Resistance

ρ: Density of conductor's material
r_v: Resistivity of the material
V: Conductor's volume
lg: Length of the conducting arm
b: Width of the conductor
d: Conductor's height.

Data Availability

The data used to support the findings of this study are available from the corresponding author upon request.

Conflicts of Interest

The authors declare that they have no conflicts of interest.

Acknowledgments

The authors want to acknowledge the Automotive Consortium for Cyber Physical Systems at Tecnológico de Monterrey and Schneider Electric for their support of this work.

References

[1] H. I. Stanback and R. H. Kingdon, Circuit Breaker, Patent 2902560, Sep. 1, 1959, US Patent Office.

[2] K. Peter Flohr, Circuit Breaker, US Patent 5565828, Oct. 15, 1996.

[3] F. L. Gelzheiser, *Circuit breaker with calibrating means*, United States Patent 4148004, Apr. 3, 1979.

[4] J. I. Melecio and H. Ahuett-Garza, "Design, Analysis, and Testing of a New Microcircuit Breaker Thermal Trip Unit Concept Based on Compliant Mechanisms," *IEEE Transactions on Industry Applications*, vol. 51, no. 4, pp. 2862–2873, 2015.

[5] H. Guckel, J. Klein, T. Christenson, K. Skrobis, M. Laudon, and E. G. Lovell, "Thermo-magnetic metal flexure actuators," in *Proceedings of the 5th IEEE Solid-State Sensor and Actuator Workshop*, pp. 73–75, June 1992.

[6] J. Jonsmann, O. Sigmund, and S. Bouwstra, "Compliant electro-thermal microactuators," in *Proceedings of the Technical Digest. IEEE International MEMS 99 Conference. Twelfth IEEE International Conference on Micro Electro Mechanical Systems (Cat. No.99CH36291)*, pp. 588–593, Orlando, FL, USA, January 1999.

[7] J. Jonsmann, O. Sigmund, and S. Bouwstra, "Compliant thermal microactuators," *Sensors and Actuators A: Physical*, vol. 76, no. 1-3, pp. 463–469, 1999.

[8] J. Luo, "Development of all metal electrothermal actuator and its applications," *Journal of Micro/Nanolithography, MEMS, and MOEMS*, vol. 4, no. 2, article 023012, 2005.

[9] K. Colbert, M. Naraghi, and J. G. Boyd, "An experimentally verified model for thermal microactuators including nonlinear material properties, vacuum, and intra-device heat conduction," *Journal of Micromechanics and Microengineering*, vol. 27, no. 2, 2017.

[10] J. Zhao, R. Gao, G. Chen, S. Liu, Q. Cao, and T. Qiu, "Nonlinear coupling mechanical model for large stroke magnetic-based multistable mechanisms," *Mechanism and Machine Theory*, vol. 83, pp. 56–68, 2015.

[11] R. Ansola, E. Veguería, J. Canales, and C. Alonso, "Evolutionary optimization of compliant mechanisms subjected to non-uniform thermal effects," *Finite Elements in Analysis and Design*, vol. 57, pp. 1–14, 2012.

[12] S. M. Lyon, P. A. Erickson, M. S. Evans, and L. L. Howell, "Prediction of the First Modal Frequency of Compliant Mechanisms Using the Pseudo-Rigid-Body Model," *Journal of Mechanical Design*, vol. 121, no. 2, p. 309, 1999.

[13] Y. Yu, L. L. Howell, C. Lusk, Y. Yue, and M. He, "Dynamic Modeling of Compliant Mechanisms Based on the Pseudo-Rigid-Body Model," *Journal of Mechanical Design*, vol. 127, no. 4, p. 760, 2005.

[14] Q. S. Xu and J. Mech, "Design, testing and precision control of a novel long-stroke flexure micropositioning system," *Mechanism and Machine Theory*, vol. 70, pp. 209–224, 2013.

[15] K.-Q. Qi, Y. Xiang, C. Fang, Y. Zhang, and C.-S. Yu, "Analysis of the displacement amplification ratio of bridge-type mechanism," *Mechanism and Machine Theory*, vol. 87, pp. 45–56, 2015.

[16] Y. Li and Q. Xu, "Design and analysis of a totally decoupled flexure-based XY parallel micromanipulator," *IEEE Transactions on Robotics*, vol. 25, no. 3, pp. 645–657, 2009.

[17] Y. Tian, B. Shirinzadeh, and D. Zhang, "Design and dynamics of a 3-DOF flexure-based parallel mechanism for micro/nano manipulation," *Microelectronic Engineering*, vol. 87, no. 2, pp. 230–241, 2010.

[18] S. Polit and J. Dong, "Development of a high-bandwidth XY nanopositioning stage for high-rate micro-/nanomanufacturing," *IEEE/ASME Transactions on Mechatronics*, vol. 16, no. 4, pp. 724–733, 2011.

[19] S. Kulkarni and S. Santoso, "Interrupting short-circuit direct current using an AC circuit breaker in series with a reactor," *Advances in Power Electronics*, vol. 2012, Article ID 805958, 14 pages, 2012.

[20] A. Mokhberdoran, A. Carvalho, N. Silva, H. Leite, and A. Carrapatoso, "Design and implementation of fast current releasing DC circuit breaker," *Electric Power Systems Research*, vol. 151, pp. 218–232, 2017.

[21] M. Deb and D. Sen, "Design of double toggle switching mechanisms," *Mechanism and Machine Theory*, vol. 71, pp. 163–190, 2014.

[22] P. Valdastri, R. J. Webster III, C. Quaglia, M. Quirini, A. Menciassi, and P. Dario, "A new mechanism for mesoscale legged locomotion in compliant tubular environments," *IEEE Transactions on Robotics*, vol. 25, no. 5, pp. 1047–1057, 2009.

[23] V. Varma and W. Dixon, "Design of a piezoelectric meso-scale mobile robot: a compliant amplification approach," in *Proceedings of the 2002 IEEE International Conference on Robotics and Automation*, pp. 1137–1142, Washington, DC, USA, 2002.

[24] P. A. York, N. T. Jafferis, and R. J. Wood, "Meso scale flextensional piezoelectric actuators," *Smart Materials and Structures*, vol. 27, no. 1, 2018.

[25] J. N. Reddy, *An Introduction to Nonlinear Finite Element Analysis*, Oxford University Press, 2004.

[26] J. I. Melecio, "Compliant Mechanisms in Miniature Circuit Breakers," *Tecnologico de Monterrey*, 2011.